Unidirectional and multi-directional wave estimation from ship motions using an Adaptive Kalman Filter with the inclusion of varying forward speed

Bourkaib, R.; Kok, M.; Seyffert, H. C.

DOI
10.1016/j.probengmech.2025.103773

Publication date
2025

Document Version
Final published version

Published in
Probabilistic Engineering Mechanics

Probabilistic Engineering Mechanics 80 (2025) 103773

Contents lists available at ScienceDirect

Probabilistic Engineering Mechanics

journal homepage: www.elsevier.com/locate/probengmech

Unidirectional and multi-directional wave estimation from ship motions using an Adaptive Kalman Filter with the inclusion of varying forward speed

R. Bourkaib [a,*], M. Kok [b], H.C. Seyffert [a]

[a] Delft University of Technology, Department of Maritime and Transport Technology, The Netherlands
[b] Delft University of Technology, Delft Center for Systems and Control, The Netherlands

ARTICLE INFO

Dataset link: 10.4121/d6e3306a-daca-4d2b-9d64-89f20e0eba5a

Keywords:
Sea state estimation
Adaptive Kalman Filter
Ship motion responses
Time domain estimation

ABSTRACT

This paper aims at estimating both unidirectional and multi-directional waves from noisy measured ship motion data, with a focus on the inclusion of the vessel's forward speed to reflect real-world operating conditions. The technique is based on an Adaptive Kalman Filter for estimating wave elevation and wave spectrum parameters, including significant wave height, peak period, and wave direction. The proposed method was tested using simulated ship motion data, and its performance was evaluated by comparing the estimated wave spectrum with reference values used in the simulation model and with results from a widely used baseline frequency domain approach. The results demonstrate that the method effectively estimates the wave spectrum in a short measuring window with a reasonable degree of accuracy when accounting for varying forward speed, indicating strong potential for real-time wave estimation to aid in improving navigation, safety, and operational efficiency.

1. Introduction

Accurate estimation of the encountered wave excitation is crucial for the safety and operational efficiency of vessels, as highlighted in several studies (e.g., [1,2]). For example, by anticipating wave patterns, operators can make real-time decisions regarding the vessel speed and heading, ensuring the ship operates within safe limits and extending its service life [3]. Accurate identification of the encountered wave energy density spectrum also allows consideration of the vessel's fatigue life consumption in comparison with the design environment [3]. These proactive measures significantly enhance both safety and operational efficiency at sea [1].

One of the most cost-effective methods for wave estimation is to consider a ship itself as a wave buoy, commonly known as the "Ship as a Wave Buoy" (SAWB) analogy [4,5]. This approach uses measurements of the ship's wave-induced motions, such as heave, pitch, and roll to estimate the encountered wave spectrum. By combining these motion measurements with a transfer function that describes the relationship between the wave input and the ship's motion response, the SAWB method provides an affordable alternative to more expensive techniques like radar [1,6] or satellite measurements.

SAWB can be performed in either the time or the frequency domain, with most previous studies focusing on the frequency domain (see e.g., [7–12]). In these studies, the energy spectrum of vessel responses is combined with Response Amplitude Operators (RAOs), linear operators describing how ship motions result from wave excitation, through spectral analysis to estimate the exciting wave spectrum. Findings indicate that this approach provides a reasonable estimate of the wave spectrum (e.g., [7,13,14]). However, the precision of the estimated spectral parameters heavily relies on a reliable RAO, which is dependent on vessel speed and loading conditions. Furthermore, this approach assumes stationary sea and vessel conditions since spectral analysis typically requires a minimum time window of 10–15 min [7]. This assumption may not hold true if the vessel speed or heading changes or if the sea state varies during the analysis period; consequently, the estimates may become unreliable [15].

To tackle these disadvantages, the time domain methods have been introduced. Based on the literature, two model types have been developed to estimate sea states in the time domain: data-driven (e.g., [16–20]) and model-based approaches, where model-based methods include a stepwise procedure (e.g., [21,22]), Kalman filtering (e.g., [23–26]), and brute-force (e.g., [27]). Both data-driven and model-based approaches have their advantages and limitations: data-driven methods need extensive data for accurate model training, whereas model-based methods depend on the precision of the RAOs and the assumption of linearity within those RAOs. For a more detailed comparison and discussion of the time-domain approaches, refer to the literature review by [28].

* Corresponding author.
E-mail address: r.b.bourkaib@tudelft.nl (R. Bourkaib).

https://doi.org/10.1016/j.probengmech.2025.103773
Received 25 February 2025; Received in revised form 22 April 2025; Accepted 6 May 2025
Available online 21 May 2025

In the context of the SAWB analogy, the Kalman Filter (KF) has proven to be both fast and capable of handling potential model inaccuracies and sensor noise [29]. Additionally, the KF is easy to implement for inverse analysis and efficient in terms of computational cost, though only a few studies have yet been performed to utilize these advantages. *Pascoal and Guedes Soares* used the KF to estimate unidirectional waves using simulated data, assuming the ship's speed to be zero [23]. They later evaluated the method with onboard ship motion measurements; however, there were limitations in identifying high-frequency waves where the ship's response is weak. Building on this work, *Kim et al.* introduced a combined approach using the KF and the Wiener filter to estimate both unidirectional and multi-directional waves using simulated ship motion data [24]. In their method, usage of the Wiener filter improved the signal-to-noise ratio, particularly in cases where the vessel acted as a low-pass filter, leading to inaccurate estimates in the high-frequency region. However, their method was limited by several restrictive conditions: the vessel's forward speed was set to zero and measurement noise characteristics were assumed to be fully known within the model. These limitations constrain the method's evaluation in real-world scenarios where varying forward speeds and unknown noise characteristics are the operational reality.

1.1. Paper objective and novelty

Usage of the Kalman filter for sea state estimation from vessel motion measurements would allow real-time estimations since only a short measuring window is needed until convergence, and it would allow fusion with other sensor sources to handle inaccuracies in measurements and model definitions. However, there is as yet no baseline Kalman filter model for inverse sea state estimation that is suited to application in real-world conditions based on non-stationary vessel conditions. In this study, we aim to address that gap by presenting an Adaptive Kalman Filter (AKF) model to estimate both unidirectional and multi-directional wave conditions from measured ship motion responses while incorporating the effects of varying forward speed and noisy measurements. The method's performance is evaluated by comparing the estimated wave spectrum parameters with reference values, assessing the accuracy of the method under realistic conditions. The method is also compared with a widely used frequency domain method [10]. It is important to note that this frequency domain method has been adapted and used as a baseline for further estimation improvements, such as using machine learning in a hybrid estimation approach [30]. Our aim here is not to evaluate the AKF approach against all possible frequency domain approaches, but to benchmark our AKF approach to the baseline frequency domain method and offer a parallel time-domain baseline.

It is further worth noting the challenge facing SAWB model-based methods regarding the use of linear RAOs. Apart from data-driven [16–20] and step-wise [21] approaches, most SAWB methods, including the one presented here, make use of linear RAOs to describe the relationship between wave excitation and wave-induced motion responses. Such an assumption proves limiting when moderate to large waves and high vessel speeds are relevant, where non-linearities and motion coupling cannot be ignored. While it is necessary to consider and model such non-linearities within the estimations for practical implementation of SAWB onboard vessels, that is beyond the scope of this current paper and is left to future work.

1.2. Paper composition

This paper is organized as follows: Section 2 outlines the methodology for wave parameter and spectrum estimation, beginning with the expressions for wave elevation and ship response. It then discusses the estimation of both unidirectional and multi-directional wave spectra using the AKF. Section 3 presents the simulation setup and results, with a focus on analyzing the effects of frequency and directional discretization. Finally, Section 4 summarizes the key findings of the study.

2. Methodology

The overall process followed for sea state estimation from ship motion measurements with the inclusion of forward speed using the AKF is illustrated in Fig. 1. First, Section 2.1 presents the wave elevation and ship response expressions that link ship motion measurements to the wave spectrum. Next, Section 2.2 describes the implementation of the AKF, including the formulation of the process and measurement models, to estimate complex wave components. Finally, Section 2.3 explains how the estimated complex wave components are used to determine key sea state parameters such as significant wave height, peak period, and mean wave direction. Note: in general the term "sea state" is used to describe encountered wave conditions, quantified by the significant wave height, peak period, and wave direction. This sea state is not to be confused with the estimated states within the AKF itself, here the complex wave components, and care is taken within the paper to distinguish these terms.

2.1. Wave elevation and ship response expressions

The wave elevation $\zeta(t)$ for unidirectional waves at time t can be described as a sum of N elementary waves as follows:

$$\zeta(t) = \sum_{i=1}^{N} A_i \cos(\omega_i t + \epsilon_i), \quad \text{with } A_i = \sqrt{2S(\omega_i)\Delta\omega_i}, \tag{1}$$

where:

- N is the total number of wave frequencies.
- A_i is the wave amplitude of the ith wave component.
- ω_i is the ith absolute wave frequency.
- ϵ_i is a random phase uniformly distributed between 0 and 2π.
- $S(\omega)$ is the unidirectional wave spectrum.
- $\Delta\omega$ is the absolute frequency interval.

For unidirectional waves, all wave energy propagates along a single direction. However, the complexity of actual ocean conditions often leads to a scenario where wave components do not uniformly travel in a single direction. This means that sea waves, in reality, are multi-directional. To accurately represent this phenomenon, the directional wave spectrum $S(\omega, \beta)$ is used, incorporating a spreading factor s that accounts for the distribution of energy across various directions. This effect is usually modeled using a spreading function $D(\beta)$, here using the Longuet-Higgins directional spreading function [31]. The directional wave spectrum is expressed as follows:

$$S(\omega, \beta) = D(\beta) \times S(\omega), \tag{2a}$$

$$D(\beta) = \frac{2^{(2s-1)} s!(s-1)!}{\pi(2s-1)!} \cos^{2s}(\beta - \bar{\beta}), \quad \text{for } |\beta - \bar{\beta}| < \frac{\pi}{2}, \tag{2b}$$

where β is the relative wave direction, $\bar{\beta}$ is the mean wave direction with reference to the vessel frame, with 180° as head seas and 0° as following seas, and s is the spreading factor which controls the width of the distribution (larger values of s indicate a more concentrated wave direction, while smaller values indicate more spread-out directions). Note that the integral of the directional spreading function over all directions should be unity because the energy remains constant before and after spreading (see, e.g., [32]). The Longuet-Higgins form for the directional spreading function was chosen for this study because it is a widely used model for representing the directional distribution of ocean waves. This form is commonly employed in wave theory, as it effectively captures the shape of wave spectra, especially in conditions where the wave energy is concentrated in specific directions.

The wave elevation for multi-directional waves at time t can then be described as follows:

$$\zeta(t) = \sum_{i=1}^{N} \sum_{j=1}^{M} A_{ij} \cos(\omega_i t + \epsilon_i) \quad \text{with } A_{ij} = \sqrt{2S(\omega_i, \beta_j)\Delta\omega_i \Delta\beta_j}, \tag{3}$$

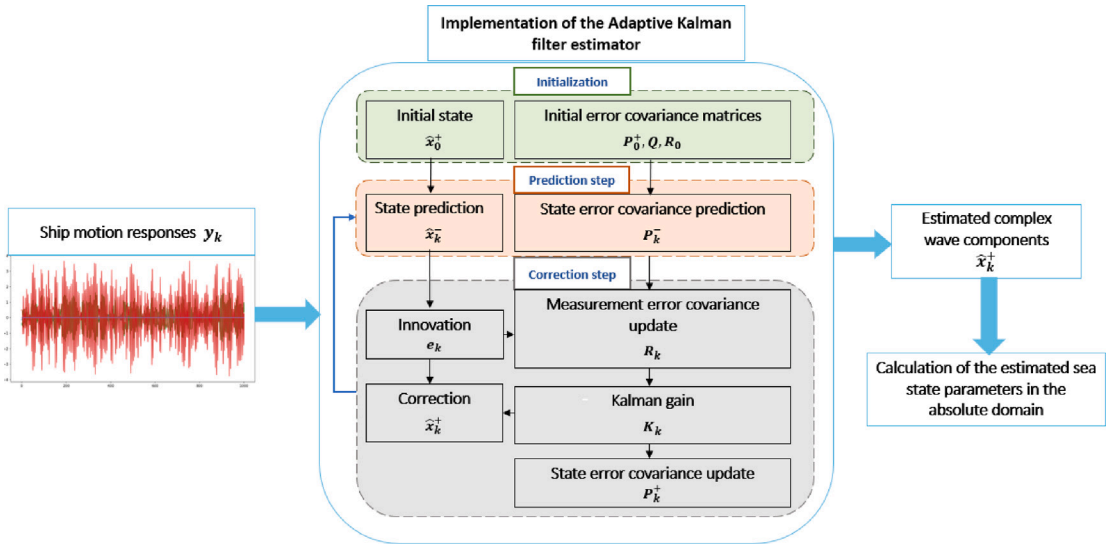

Fig. 1. Process of sea state estimation from ship motion measurements using the AKF.

where $\Delta\beta$ and M represent the relative wave direction interval and the total number of relative wave directions, respectively. A_{ij} represents the wave amplitude for the ith frequency and the jth direction.

We further consider a ship with non-zero forward speed U. To account for this, both the wave spectrum and the wave frequency must be transformed from the absolute to the encounter domain, as outlined by [33]. This transformation accounts for the relative motion between the vessel and the waves, influenced by the Doppler shift effect, and adjusts the absolute wave frequencies accordingly. The mapping of the absolute frequency ω to the encounter frequency ω_e is expressed by Eq. (4a). Additionally, the encounter wave spectrum $S(\omega_e)$ is calculated using the derivative of Eq. (4a) with respect to ω, and using Eq. (4b), as shown in Eq. (4c). Here Eq. (4b) represents the energy equivalence theorem, which ensures that the energy is conserved between the absolute wave spectrum and the encounter wave spectrum.

$$\omega_e = \omega - \omega^2\psi, \quad \text{with } \psi = \frac{U}{g}\cos(\beta), \tag{4a}$$

$$S(\omega_e)\Delta\omega_e = S(\omega)\Delta\omega, \tag{4b}$$

$$S(\omega_e) = S(\omega)\frac{1}{1-2\omega\psi}, \tag{4c}$$

where g is the acceleration due to gravity. Therefore, the wave elevation described by Eq. (3) can be refined to include the effects of the ship's forward speed, as follows:

$$\zeta(t) = \sum_{i=1}^{N}\sum_{j=1}^{M} A_{e,ij}\cos(\omega_{e,i}t+\epsilon_i), \quad \text{with } A_{e,ij} = \sqrt{2S(\omega_{e,i},\beta_j)\Delta\omega_{e,i}\Delta\beta_j}, \tag{5}$$

where $\Delta\omega_{e,i}$ is the encounter frequency interval.

To calculate a vessel's lth degree of freedom (DOF) response to the defined wave elevation (where l represents the DOF of the vessel's motion, such as surge, heave, pitch, or roll), the linear RAO model, which characterizes the vessel's response to incoming waves, is applied. This RAO is complex, comprising both amplitude and phase components, and is a function of the degree of freedom l, wave frequency i, and wave direction j. The RAO amplitude and RAO phase can be determined via:

$$|\mathrm{RAO}_{lij}| = \sqrt{\mathrm{Re}(\mathrm{RAO}_{lij})^2 + \mathrm{Im}(\mathrm{RAO}_{lij})^2}, \tag{6a}$$

$$\varphi_{lij} = \tan^{-1}\frac{\mathrm{Im}(\mathrm{RAO}_{lij})}{\mathrm{Re}(\mathrm{RAO}_{lij})}, \tag{6b}$$

where $\mathrm{Re}(\mathrm{RAO}_{lij})$ and $\mathrm{Im}(\mathrm{RAO}_{lij})$ represent the real and the imaginary parts of the RAO model, respectively.

The vessel's lth DOF motion response accounting for forward speed is then obtained by multiplying the wave elevation described in Eq. (5) with the complex RAO model, as shown below:

$$y_l(t) = \sum_{i=1}^{N}\sum_{j=1}^{M} \mathrm{RAO}_{lij} \times A_{e,ij}\cos(\omega_{e,i}t+\epsilon_i), \tag{7}$$

where RAO_{lij} is the complex RAO model for the lth DOF. Note that the RAO model is dependent on the vessel speed and loading condition.

In order to represent Eq. (7) with respect to the complex wave components, which represent the states within the AKF to be estimated, we decompose it into its quadrature components, as outlined by [23]. Then Eq. (7) becomes:

$$y_l(t) = \sum_{i=1}^{N}\sum_{j=1}^{M} \mathrm{RAO}_{lij} \times (x_{1,ij}\cos(\omega_{e,ij}t) + x_{2,ij}\sin(\omega_{e,ij}t)), \tag{8}$$

where $x_{1,ij} = A_{e,ij}\cos(\epsilon_i)$ and $x_{2,ij} = -A_{e,ij}\sin(\epsilon_i)$ represent the real and imaginary components of the complex wave for the ith frequency and jth direction, respectively.

Rewriting Eq. (8) using the magnitude and phase of the RAO results in:

$$\begin{aligned} y_l(t) = &\sum_{i=1}^{N}\sum_{j=1}^{M} |\mathrm{RAO}_{lij}|\cos(\omega_{e,i}t + \varphi_{lij})x_{1,ij} \\ &+ \sum_{i=1}^{N}\sum_{j=1}^{M} |\mathrm{RAO}_{lij}|\sin(\omega_{e,i}t + \varphi_{lij})x_{2,ij}, \end{aligned} \tag{9}$$

Finally, Eq. (9) will be used in the measurement model of the KF, as further described in Section 2.2.

2.2. Adaptive Kalman filter implementation

The KF is a recursive algorithm widely used in various applications for reliable state estimation [34]. To implement the filter, it is essential to first establish a state-space model. This model includes a process model, which describes the evolution of the states we aim to estimate over time, and a measurement model, which relates the observed data to the states. Additionally, the uncertainties in both the system dynamics and measurements are accounted for and are modeled as Gaussian using covariance matrices for process and measurement noise.

In this study, we use the KF to estimate the system states, specifically complex wave components, from noisy ship motion measurements. The process model equation can be represented as follows:

$$x_{k+1} = \phi_k x_k + w_k, \quad \text{with } w_k \sim \mathcal{N}(0, Q), \tag{10}$$

where:

- $x_k = [x_{1,ij} \cdots x_{1,NM}, x_{2,ij} \cdots x_{2,NM}]^T$ is the state vector at time instance k of the complex wave components with dimension $2NM$.
- x_{k+1} is the state vector at the next time instant.
- ϕ is the transition matrix with dimension $2NM \times 2NM$. It is an identity matrix as the sea state is assumed to be stationary within a given time window.
- w_k is the $2NM$ dimensional process noise vector.
- $\mathcal{N}(0, Q)$ is a normal distribution with zero mean and a process covariance error Q.

Based on Eq. (9), the measurement model in discrete time for the wave-induced ship responses can be expressed as follows:

$$y_k = H_k x_k + v_k, \quad \text{with } v_k \sim \mathcal{N}(0, R_k), \tag{11}$$

where:

$$H_k = \begin{bmatrix} C_{111} & \cdots & C_{1ij} & \cdots & C_{1NM} & S_{111} & \cdots & S_{1ij} & \cdots & S_{1NM} \\ \vdots & \ddots & \vdots & \ddots & \vdots & \vdots & \ddots & \vdots & \ddots & \vdots \\ C_{L11} & \cdots & C_{Lij} & \cdots & C_{LNM} & S_{L11} & \cdots & S_{Lij} & \cdots & S_{LNM} \end{bmatrix}, \tag{12}$$

with:

$$C_{lij} = |\mathrm{RAO}_{lij}| \cos(\omega_{e,i} k \Delta t + \varphi_{lij}),$$

$$S_{lij} = |\mathrm{RAO}_{lij}| \sin(\omega_{e,i} k \Delta t + \varphi_{lij}).$$

- L is the number of vessel responses used in the KF technique.
- y_k is the $L-$dimensional ship motion measurement vector at time k.
- x_k is the state vector with dimension $2NM$.
- v_k is the $L-$dimensional measurement noise vector with zero mean and covariance R_k.
- k is the number of the time step.
- Δt is the time interval.

After formulating the process and measurement models, the state vector x_k can be estimated from ship motion measurements y_k. This estimation is carried out in three main steps (see Fig. 1): initialization, prediction, and correction.

2.2.1. Initialization

In the initialization step, at $k = 0$, the initial state $\hat{x}_0^+$ is set. Since no prior knowledge of $\hat{x}_0^+$ is available, it is initialized to zero. Additionally, since the sensor noise is unknown to the model and may vary due to changes in the ship's forward speed, the measurement error covariance matrix R_k is adaptively estimated (see Eq. (14b)). Instead of using a constant R_k, it is estimated through innovation-based adaptive estimation [34]. On the other hand, the process error covariance matrix Q is fixed through a tuning process. The AKF assumes independent, identically (Gaussian) distributed noise, and can handle the noise well with proper tuning of the measurement noise covariance, such as in this case, although performance will of course degrade for larger noise covariances. However, if the noise is non-Gaussian and the signal contains outliers, this will degrade the filter's performance. This could be mitigated by using pre-processing techniques like removing outliers or applying band-pass filtering to remove high-frequency noise before passing the measurements to the Kalman filter, but that is considered to be outside the scope of this work. Such techniques are especially important when working with real (instead of simulated) data. Or if the noise has known (but still non-Gaussian) characteristics, e.g., a bias, this can be dealt with by, e.g., an offset within the process model.

Note that to mitigate the overestimation at high wave frequencies where the ship response is weak (as seen by, e.g., [35]), we assign low Q values to these high wave frequencies compared to the other frequencies; the cut-off for defining "high wave frequencies" is based on where the RAO amplitudes tend to negligible responses. We set a large initial state error covariance P_0 to account for uncertainty between the estimated and the ground truth state at $k = 0$. Since the ground truth is unknown, we set $x_0 = 0$ and P_0 large enough to account for this uncertainty. However, similar to Q, we adjust P_0 based on wave frequency to ensure the initial state uncertainty aligns with the expected dynamics. To determine the most effective implementation, we tested both a strict division where a fixed cut-off frequency separates high and low wave frequencies and a smooth transition using a sliding scale. Since both approaches gave similar results, we opted for the strict division for its simplicity. Additionally, we compared this approach with the Wiener filter-based method proposed by [24] and found that assigning low Q values to high wave frequencies achieved a similar objective. However, our approach is simpler to implement, as it only requires adjusting Q and P_0 rather than modifying the RAO model itself. This adjustment of Q and P_0 also indicates how the noise intensity affects the model performance: when the signal-to-noise ratio is low (such as the low motion responses in high frequencies), the model estimation can suffer, and some adjustment of the model may be necessary to improve estimation accuracy.

2.2.2. Prediction

In the prediction step, the current state $\hat{x}_k^-$ is predicted from the previous estimated state $\hat{x}_k^+$ using the state transition matrix ϕ_k (see Eq. (13a)). The uncertainty in this prediction, P_k^-, is calculated using the process error covariance Q (see Eq. (13b)).

$$\hat{x}_k^- = \phi_k \hat{x}_k^+, \tag{13a}$$

$$P_k^- = \phi_k P_k^+ \phi_k^T + Q. \tag{13b}$$

2.2.3. Correction

In the correction step, the predicted state $\hat{x}_k^-$ and its corresponding covariance P_k^- are updated using the error between the current ship motion measurements and the predicted measurements, weighted by the Kalman gain K_k (see Eqs. (14e) and (14f)), to obtain a more accurate estimate. The Kalman gain, defined in Eq. (14d), optimally balances the predicted state with the observed measurement data, minimizing the estimation error. The $\hat{x}_k^+$ and P_k^+ are then used for the next prediction cycle.

$$\text{Innovation:} \quad e_k = y_k - H_k \hat{x}_k^- \tag{14a}$$

$$\text{Updated measurement error covariance:} \quad R_k = \alpha R_{k-1} + (1-\alpha)(e_k e_k^T - H_k P_k^- H_k^T) \tag{14b}$$

$$\text{Innovation covariance:} \quad S_k = H_k P_k^- H_k^T + R_k \tag{14c}$$

$$\text{Kalman gain:} \quad K_k = P_k^- H_k^T S_k^{-1} \tag{14d}$$

$$\text{Updated state:} \quad \hat{x}_k^+ = \hat{x}_k^- + K_k e_k \tag{14e}$$

$$\text{Updated state covariance:} \quad P_k^+ = (I - K_k H_k) P_k^- \tag{14f}$$

In Eq. (14b), α is a smoothing factor that determines how much weight is given to the previous R_k; it is chosen between 0 and 1. The size of the AKF matrices for multi-directional wave estimation are given in Table 1. For unidirectional wave estimation, note that $M = 1$, as the wave direction is assumed to be known.

Finally, the AKF continuously improves the accuracy of the state estimates within a stationary window, making it effective in handling Gaussian noise or incomplete data.

2.3. Wave spectrum and parameter calculation

After estimating the complex wave components $\hat{x}_k^+$ using the AKF, we calculate the wave elevation and the spectral parameters based on those estimates as follows:

Table 1
Variables and their dimensions in the AKF model for multi-directional wave estimation.

Variable	Description	No. of rows	No. of columns
x_k	State vector	$2NM$	1
y_k	Measurement vector	L	1
ϕ	State transition matrix	$2NM$	$2NM$
H_k	Output matrix	L	$2NM$
P_k	State covariance matrix	$2NM$	$2NM$
K_k	Kalman gain matrix	$2NM$	L
Q	Process error covariance matrix	$2NM$	$2NM$
R_k	Measurement error covariance matrix	L	L

- **Estimated encounter wave spectrum:** This can be determined using the estimated complex wave components by:

$$S(\omega_{e,i},\beta_j)=\frac{1}{2\Delta\omega_{e,i}\Delta\beta_j}\times(\hat{x}^{+2}_{1,ij}+\hat{x}^{+2}_{2,ij}), \tag{15}$$

where $\hat{x}^{+2}_{1,ij}$ and $\hat{x}^{+2}_{2,ij}$ represent the estimated real and imaginary complex wave components of the ith encounter frequency of the jth relative wave direction, respectively. Note that for unidirectional waves, where β is fixed, the term $\Delta\beta_j$ is removed as the wave energy is assumed to propagate in a single direction.

- **Estimated absolute wave frequency and spectrum:** The transformation between the absolute frequency domain and the encounter frequency domain is controlled by the Doppler shift, as described by Eq. (4a). This process varies with relative wave direction and ship speed. In head sea conditions, the transformation is straightforward (each encounter frequency directly matches a single absolute frequency). However, for following seas when the encounter frequencies are below a certain threshold ($\omega_e < 1/4\psi$), the transformation becomes complex, as one encounter frequency can correspond to three absolute frequencies, as demonstrated by [33].

Subsequently, the transformation of the wave energy spectrum from the encounter domain to the absolute domain relies on the fact that the energy must be conserved, as shown in Eq. (4b). In this case, the absolute wave spectrum for unidirectional waves can be estimated based on Eqs. (4a) and (4b), as follows:

$$S(\omega)=S_e(\omega_e)\frac{\Delta\omega_e}{\Delta\omega}=S_e(\omega_e)(1-2\omega\psi). \tag{16}$$

For the multi-directional waves, the estimated absolute wave spectrum can be calculated using the following formula:

$$S(\omega,\beta)=S_e(\omega_e,\beta)(1-2\omega\psi). \tag{17}$$

It is important to note that under head sea conditions, Eq. (17) can be used directly to calculate the absolute wave spectrum. However, in following/ stern-quartering seas, a more complex approach is required, as there is no unique transformation solution, and the encounter frequency domain must be mapped to three corresponding ordinates in the absolute wave-frequency domain. For a detailed explanation of this method, refer to [33]. In the current paper following seas are not considered.

- **Estimated mean wave direction:** For multi-directional waves, the estimated mean direction can be determined using the following formula:

$$\bar{\beta}=\arctan\left(\frac{d}{c}\right), \tag{18}$$

where:

$$c=\int_{-\pi}^{\pi}\int_{0}^{\infty}S(\omega,\beta)\cos(\beta)\,d\omega\,d\beta, \tag{19}$$

$$d=\int_{-\pi}^{\pi}\int_{0}^{\infty}S(\omega,\beta)\sin(\beta)\,d\omega\,d\beta. \tag{20}$$

Fig. 2. USCGC STRATTON [36].

- **Estimated significant wave height:** This can be calculated either from the estimated encounter wave spectrum or absolute wave spectrum, as energy must be conserved in both domains. The significant wave height can also be calculated from the wave elevation:

$$M_0=\int S_e(\omega_e)d\omega_e=\int S(\omega)d\omega, \tag{21a}$$

$$H_s=4\sqrt{M_0}=4\times\sigma, \tag{21b}$$

where M_0 represents the zeroth spectral moment of the estimated wave energy and σ is the standard deviation of the estimated wave elevation $\xi(t)$. Note that for the multi-directional case, $S(\omega)$ is obtained by integrating $S(\omega,\beta)$ over β.

- **Estimated peak period:** This is estimated from the peak of the calculated absolute wave spectrum.

$$\omega_p=\text{argmax}(S(\omega)), \tag{22a}$$

$$T_p=\frac{2\pi}{\omega_p}, \tag{22b}$$

where ω_p represents the angular frequency corresponding to the maximum amplitude in the estimated wave spectrum.

- **Estimated wave elevation**: This can be estimated as follows:

$$\xi(t)=[\cos(\omega_{e,11}t),\dots,\cos(\omega_{e,NM}t),\ \sin(\omega_{e,11}t),\dots,\sin(\omega_{e,NM}t)]\cdot[\hat{x}^{+}_{1,11},\dots,\hat{x}^{+}_{1,NM},\hat{x}^{+}_{2,11},\dots,\hat{x}^{+}_{2,NM}]^T. \tag{23}$$

3. Case study and discussion

The proposed method for wave spectrum estimation from measured ship motion responses with the inclusion of forward speed was tested using synthetic ship motion data. The measurements used in the AKF are surge, sway, heave, roll, and pitch motions. The model of the United States Coast Guard Cutter (USCGC) STRATTON was employed, as illustrated in Fig. 2. Table 2 specifies the ship's dimensions. The RAOs for this vessel at different forward speeds were provided by the Maritime Research Institute Netherlands (MARIN), which has carried out extensive monitoring campaigns for this vessel (see, e.g., [36,37]).

3.1. Simulation details

The simulated ship motion responses for unidirectional waves were generated using Eq. (7), and multi-directional waves were generated using the equal energy method instead of the traditional double sum method commonly used in the literature [24,38]. The equal energy method was chosen to ensure a more accurate representation of the

Table 2
Main particulars of the vessel [37].

Main particular	Ft/m
Length overall	418.60 ft/127.29 m
Length between perpendiculars	390.00 ft/118.87 m
Beam, waterline	48.89 ft /14.9 m
Beam, maximum	54.00 ft/16.46 m
Design draft	14.40 ft/4.39 m
Block coefficient	0.492/0.492
Displacement (fully appended)	4500 LT/4571 tonnes

random ergodic nature of ocean waves, which are stationary and homogeneous for limited time durations [39]. The double sum method does not provide an ergodic solution due to interactions between waves of the same frequency but in different directions. By using the equal energy method, wave energy is uniformly distributed across all frequencies and directions, overcoming this limitation.

The lth motion response at a given point (x, y) can be described using the equal energy method as follows:

$$y_l(x,y,t) = \sum_{i=1}^{N} \sqrt{2|\mathrm{RAO}_{li}|^2 S(\omega_{\mathrm{e},i})\Delta\omega_{\mathrm{e},i}}\cos(\omega_{\mathrm{e},i}t - \kappa_i(x\cos(\beta_i) + y\sin(\beta_i)) + \epsilon_i + \varphi_{li}), \tag{24}$$

where:

- κ_i is the wave number.
- β_i is the random direction vector, determined using the equal energy method. In this method, the directional spreading function is used as a probability density function to assign a propagation direction to each wave component. For a detailed description of the procedures followed, refer to [40].

The simulations focused on estimating various sea states, as further described in Sections 3.2–3.3. A JONSWAP wave spectrum was employed with a peak enhancement parameter γ of 3.3 to simulate the waves [41]. To avoid repetition effects after $2\pi/\Delta\omega_{\mathrm{e}}$, a large number of frequencies (500) were used to generate the ship motions. Sensor noise with a signal-to-noise ratio of 20 was added to the simulated response motions to closely simulate real-world conditions; note that the sensor noise description was still considered as an unknown within the AKF implementation. The encounter wave frequency ω_{e} was used instead of the absolute frequency ω to account for the ship's forward speed. Multiple cases, where the ship is moving with a constant forward speed, 9.26 m/s (18 kts), 14.4 m/s (28 kts), or a varying one, decreasing from 9.26 m/s to 5 m/s over the last 400 s, were analyzed to evaluate the impact of (varying) speed on the estimation process. The method was also tested for other forward speeds with a Froude number below 0.42 to ensure its applicability. Note that when we choose a forward speed with a Froude number higher than 0.3, the nonlinear effects become significant, and adjustments to the ship model may be required.

The AKF was applied using the simulated ship motion responses. The number of encounter frequencies N and the encounter frequency interval $\Delta\omega_{\mathrm{e}}$ used in the output matrix of the AKF were determined through a series of numerical experiments to assess the filter's effectiveness in estimating the wave spectrum. It is important to note that selecting a small $\Delta\omega_{\mathrm{e}}$ results in a larger number of complex wave components to estimate, as its size is $2NM$. As a result, the number of unknown parameters increases, which can reduce the filter's accuracy due to the added complexity. Therefore, finding the optimal number of frequencies is critical for ensuring accurate wave spectrum estimation. The values of AKF parameters are given in Table 3, where I is the identity matrix with the dimension in Table 1.

3.2. Unidirectional waves

From Eq. (15), the encounter unidirectional wave spectrum is determined by averaging the estimated wave components over the 500 last seconds. This approach smooths out short-term fluctuations, making it easier to compare theoretical predictions with the inverse estimation results. Then, the estimated absolute wave spectrum is obtained using the transformation from encounter to absolute domain via Eq. (17).

Fig. 3 compares the simulated and estimated absolute wave spectra for unidirectional waves, corresponding to a significant wave height of 3 m and a peak period of 9 s, with the relative direction of 180° (case 2 in Table 4). The figure shows two estimation results: one using a uniform Q across all frequencies and another using the modified, non-uniform Q which has lower values at high frequencies ($\omega > 1.15$ rad/s), first introduced in Section 2.2.1. We notice that there is an overestimation at high frequencies when a uniform Q is applied (blue line in Fig. 3). This is because the vessel motion RAO amplitudes tend to zero at higher wave frequencies, causing sensor noise in the measured signal to be amplified. In contrast, assigning lower values to Q for high frequencies (orange line in Fig. 3) effectively mitigates the high-frequency overestimation, preventing the divergence observed by [35].

When using this modified, non-uniform Q, we observe that the estimated absolute wave spectrum closely aligns with the simulated spectrum across a range of frequencies, demonstrating the robustness of the estimation process, especially at lower frequencies where wave energy is concentrated. However, some underestimation does occur in certain areas, likely due to the filter's limitations with non-matching frequencies. Specifically, the output matrix of the AKF is based on frequencies that do not perfectly match those of the original motion signal. This mismatch occurs because these frequencies are unknown, adding complexity to the estimation process.

Increasing the number of frequencies to address the underestimation is not a viable solution, as it introduces more unknown parameters, and consequently, the filter may not perform well under these conditions. Thus, after a series of numerical experiments, a sampling frequency of 0.02 rad/s was selected. The estimated spectrum obtained with this sampling frequency provides a satisfactory balance between minimizing underestimation and maintaining overall accuracy.

Based on the estimated complex wave components, the wave elevation was obtained using Eq. (23). Fig. 4 presents both the simulated and estimated wave elevations for the last 100 s of the simulation. The figure shows that the simulated and estimated wave elevation are in good agreement with a correlation of 0.89, demonstrating the accuracy of the estimation method.

Based on the estimated wave spectrum, the significant wave height and peak period were evaluated over time, as shown in Figs. 5(a) and 5(b). The estimated parameters start converging to the simulated values around 300 s and thereafter of the simulation time. This effective convergence demonstrates that the AKF becomes more accurate and stable over time and further indicates the short measurement windows required for implementing the AKF for inverse wave estimation.

Fig. 6 presents the simulated heave motion before the addition of measurement noise, and the heave motion predicted by the AKF. The figure shows that the predicted motion aligns closely with the simulated motion, with a correlation of 0.96. This observation suggests that the AKF effectively captures the motion dynamics and is able to filter out the added noise.

The proposed method was evaluated for various unidirectional wave scenarios under different ship forward speeds, both constant and varying, as indicated in Table 4. This table represents the simulated and estimated sea state parameters (significant wave height H_{s} and peak period T_{p}). In terms of errors, significant wave height error ranges from 0.23 m to 0.76 m, while peak wave period errors range from 0.37 s to 0.76 s. Despite these errors, there is generally good agreement

Table 3
AKF parameters values used in the estimation of unidirectional waves and multi-directional waves.

AKF parameters	Unidirectional waves	Multi-directional waves
Number of encounter wave frequencies N	99	40
Frequency range ω [rad/s]	$[0.02, 2]$	$[0.05, 2]$
Relative wave direction range β [deg]	–	$[90, 280]$
Motion time length t [s]	1000	1000
Sampling time Δt [s]	0.1	0.1
Initial state vector x_k	0	0
Initial state error covariance P_0	Diagonal values: 10, with lower values of 1 at high frequencies	Diagonal values: 10, with lower values of 1 at high frequencies
Initial measurement error covariance R_0	Diagonal values: 10^{-2} for translational motions and 10^{-3} for rotational motions	Diagonal values: 10^{-2} for translational motions and 10^{-3} for rotational motions
Process error covariance Q	Diagonal values: 0.01, with lower values of 0.001 at high frequencies	Diagonal values: 0.1, with lower values of 0.01 at high frequencies

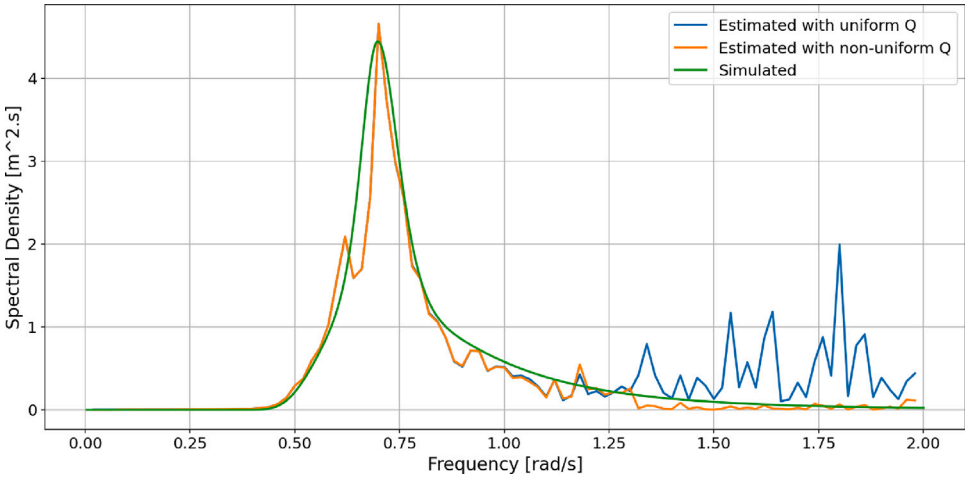

Fig. 3. Simulated and estimated absolute wave spectrum with the uniform and non-uniform Q for case 2 (see Table 4). (For interpretation of the references to color in this figure legend, the reader is referred to the web version of this article.)

Table 4
Comparison of simulated and AKF-estimated sea state parameters for unidirectional wave cases. Note that $H_s(=4\sigma)$ is generated two ways: from the wave spectrum and from the wave elevation time series in parenthesis.

Case No.	Forward speed	Simulated sea parameters			AKF-Estimated sea parameters	
	U [m/s]	H_s [m]	T_p [s]	$\bar{\beta}$ [deg]	H_s [m]	T_p [s]
1	9.26	4.97 (4.97)	9.00	180	4.50 (4.65)	9.23
2	9.26	3.99 (3.99)	9.00	180	3.67 (3.67)	8.97
3	9.26	3.99 (3.99)	9.00	210	3.71 (3.82)	9.23
4	14.40	3.99 (3.99)	9.00	180	3.73 (3.55)	8.97
5	From 9.26 to 5	4.97 (4.97)	8.99	180	4.45 (4.40)	9.67

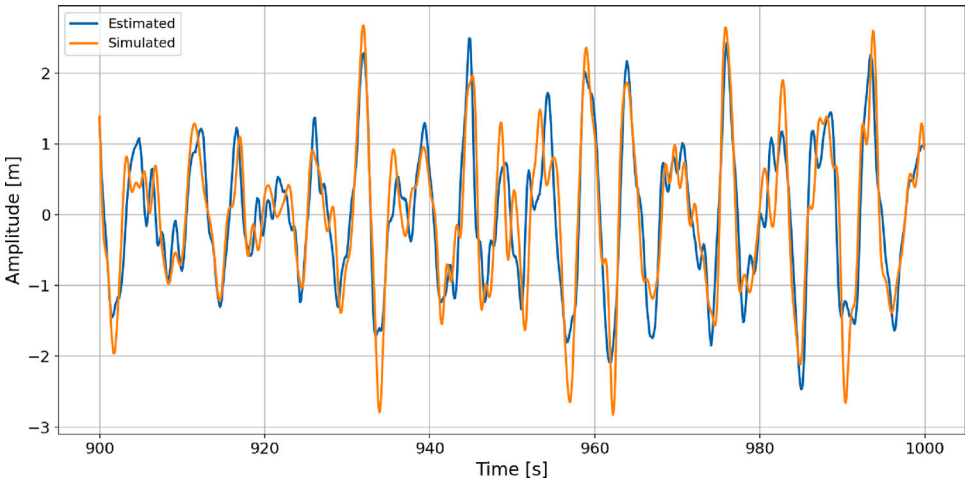

Fig. 4. Simulated and estimated wave elevation for unidirectional waves case 2 (see Table 4).

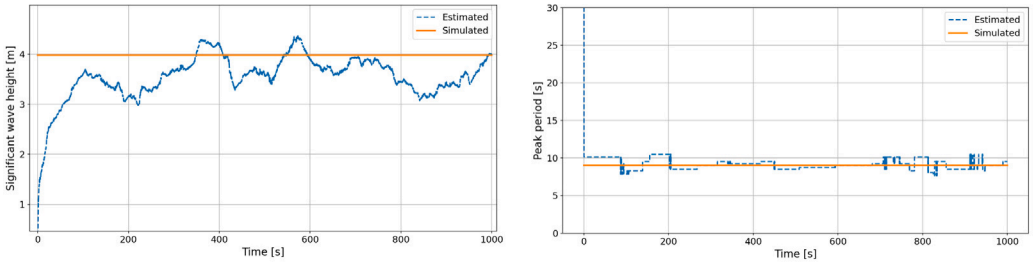

(a) Significant wave height. (b) Peak period.

Fig. 5. Simulated and estimated sea state parameters over time for unidirectional waves case 2 (see Table 4).

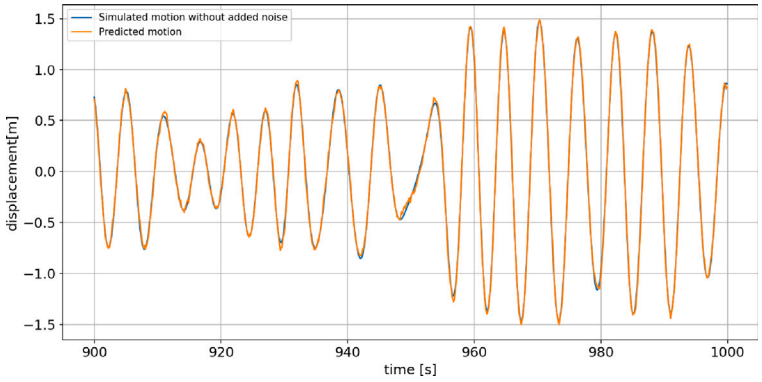

Fig. 6. Simulated and estimated heave motion response for unidirectional waves case 2 (see Table 4).

between the estimated wave spectral parameters and the simulated spectral parameters across different sea states. This overall alignment suggests that the proposed method is reliable and effective in various sea conditions. Additionally, the results obtained for Case 5, which involved changes in the ship's forward speed, indicate that the method performs well under non-stationary ship conditions.

Compared to existing work that focuses on estimating wave spectral parameters from ship motion responses in the time domain [23,24], the proposed method achieves a similar level of accuracy while additionally accounting for the challenges of forward speed and unknown measurement noise, which are not considered in those works.

3.3. Multi-directional waves

The proposed AKF approach was also tested for multi-directional seas, where the estimated wave spectra were determined using the equations described in Section 2. Here, the directional spreading factor s from Eq. (2b) is set to 2 to simulate moderate directional wave spreading, which is common in real-world scenarios; the wave energy is moderately concentrated around the peak direction but with some spread.

Fig. 7 illustrates the simulated and estimated absolute overall wave spectra corresponding to case 1 ($H_s = 5$ m, $T_p = 9$ s and $\bar{\beta} = 180°$), where the ship forward speed is 9.26 m/s (18 kts). We observe that the estimated absolute wave spectrum closely matches the original spectrum, demonstrating the effectiveness of the proposed method. However, similar to the unidirectional wave estimation, some underestimation is observed due to the AKF's challenges with non-matching frequencies and the increased number of unknown parameters in the multi-directional case, which adds complexity to the estimation process. Additionally, assigning lower Q values at high frequencies effectively addresses the divergence in the high-frequency spectrum, as no overestimation is observed in this range ($\omega > 1.15$ rad/s).

The polar plots shown in Fig. 8 represent the simulated and estimated directional wave spectrum for case 2 ($H_s = 5$ m, $T_p = 9$ s and $\bar{\beta} = 180°$), where the ship forward speed is 9.26 m/s (18 kts). From Fig. 8(b), we observe that the wave energy is concentrated primarily around 180°, which indicates that the majority of wave energy is coming from this direction. This concentration aligns with the simulated mean wave direction in this particular case, as shown in Fig. 8(a). For this multi-directional wave estimation, we observe a discrepancy in the wave directional distribution, as seen in Fig. 8(b), where the estimated distribution appears asymmetric, while the simulated wave data are symmetrically distributed. This discrepancy could be attributed to the discretization of both the frequency and direction in the model. In other words, the way the wave directions and frequencies are discretized might not be fine enough to fully capture the complexity of the wave field, leading to some directions being either overestimated or underestimated. Additionally, the fact that we are estimating a large number of states compared to the available measurements may affect the accuracy of the estimation. Another important note is that the AKF does not assume a shape or symmetry of the estimated wave spectrum, so we do not necessarily expect a symmetric spectrum estimation based on the known limitations discussed above. As a point of future work to improve the estimation, we propose to use more measurements, such as radar data, which can provide accurate information about wave directionality and may help correct asymmetries in the wave spectrum by adding more reliable directional data.

Further, for the multi-directional case, the estimated wave elevation aligns reasonably well with the simulated wave elevation, as shown in Fig. 9. However, some underestimation or overestimation of the wave elevation is observed, which can be attributed to the increased number of parameters due to a larger range of directions and frequencies, which introduces further complexity.

The estimated significant wave height and peak period were evaluated over time, as shown in Figs. 10(a) and 10(b). The estimated parameters oscillate around the original wave parameters at approximately 400 s and throughout the remainder of the simulation. This effective convergence demonstrates that the AKF is accurate and stable over time.

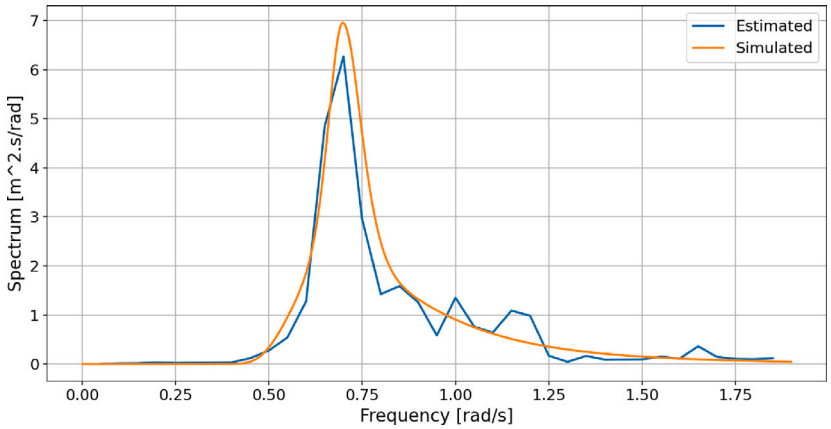

Fig. 7. Simulated and estimated wave spectrum for multi-directional waves case 1 (see Table 5).

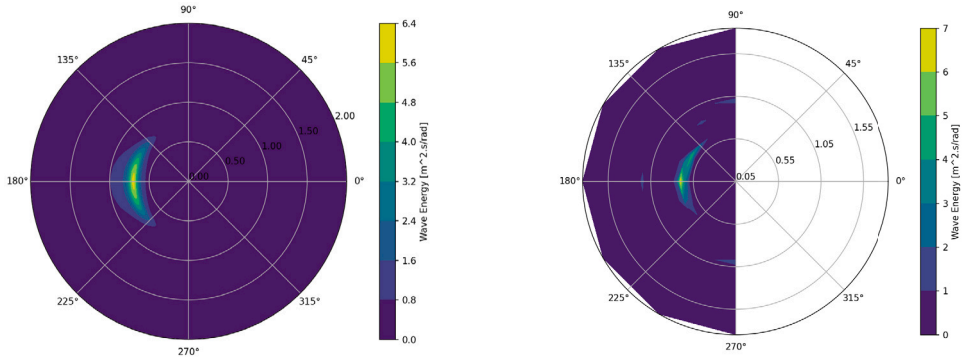

(a) Simulated. (b) Estimated.

Fig. 8. Simulated and estimated polar plot of directional wave spectrum case 1 (see Table 5).

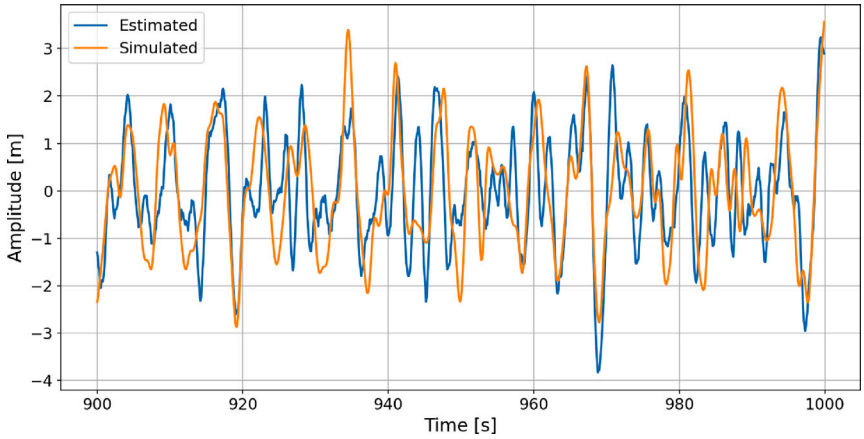

Fig. 9. Simulated and estimated wave elevation for multi-directional waves case 1 (see Table 5).

The proposed method was evaluated for various multi-directional wave scenarios under different ship forward speeds, both constant or varying, as described in Table 5. This table represents the estimated sea state parameters (significant wave height H_s, peak period T_p, and mean direction $\bar{\beta}$) obtained from the AKF and the baseline frequency domain method from [10].

In general, both the AKF and the baseline frequency domain method estimate the significant wave height close to the simulated value, with the AKF estimates for a deviation of 0.27 m to 0.63 m, the peak period with a deviation of about 0.1 s to 0.6 s, and the mean direction of about 0.6°. The baseline frequency domain method's estimates show similar accuracy. The AKF approach introduced here gives similar results to the baseline frequency domain method but is easier to implement, requires less simulation time to convergence of sea state parameters (~8 min vs. 10–15 min), and needs fewer assumptions for implementation, making it better suited for real-time applications with limited resources. Additionally, the AKF can estimate the wave spectrum even when the forward speed varies, as demonstrated by Case 5, making it suitable for dynamic conditions. However, the baseline frequency domain method assumes stationary conditions, which limits its ability to handle changes in forward speed effectively.

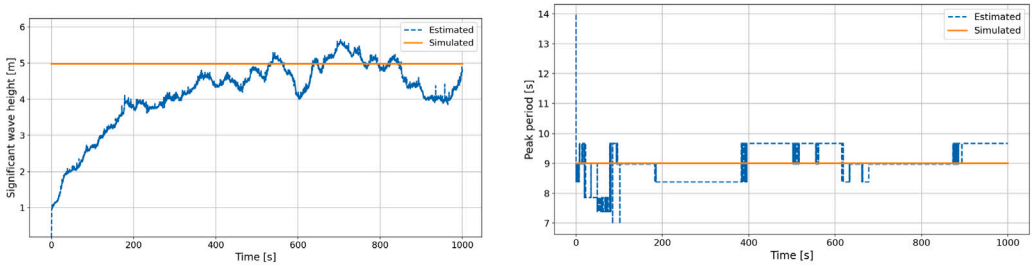

(a) Significant wave height. (b) Peak period.

Fig. 10. Simulated and estimated sea state parameters over time for multi-directional waves case 1 (see Table 5).

Table 5
Comparison of simulated and estimated wave spectrum parameters for multi-directional cases from the AKF and the baseline frequency domain (Baseline FD) method from [10]. Note that $H_s(=4\sigma)$ is generated two ways: from the wave energy spectrum, and from the generated/estimated wave elevation time series in parenthesis.

Case No.	Forward speed	Simulated sea parameters			Estimated sea parameters					
					AKF			Baseline FD		
	U [m/s]	H_s [m]	T_p [s]	$\bar{\beta}$ [deg]	H_s [m]	T_p [s]	$\bar{\beta}$ [deg]	H_s [m]	T_p [s]	$\bar{\beta}$ [deg]
1	9.26	4.97 (4.97)	9.03	180	4.73 (4.39)	8.97	180.46	5.40	8.97	178.65
2	9.26	3.99 (3.99)	9.03	180	3.76 (3.52)	9.66	179.06	3.67	8.97	179.72
3	9.26	3.99 (3.99)	9.03	210	4.04 (3.64)	9.66	201.24	4.21	8.97	194.27
4	14.40	3.99 (3.99)	9.03	180	3.36 (3.65)	9.66	182.10	3.67	8.97	179.72
5	From 9.26 to 5	4.97 (4.97)	9.03	180	4.47 (4.49)	8.76	179.66	–	–	–

4. Conclusions

In conclusion, this paper presented a method using the AKF for estimating both unidirectional and multi-directional wave spectra based on vessel motion measurements with unknown Gaussian noise and the inclusion of forward vessel speed. Simulation results showed that the method accurately estimates wave parameters under real-world conditions, where the ship's forward speed may vary, and it achieves almost the same degree of precision as existing techniques assuming either zero or constant forward speed [23–25,42]. To overcome the issue of overestimation at higher wave frequencies, we introduced the application of low Q and P_0 at high wave frequencies. This reduces the filter's sensitivity to high-frequency components, which are more prone to noise. The ship's motion responses were generated using the equal-energy method to ensure ergodicity, and a wide range of frequencies was used to avoid repetition of the signal after $2\pi/\Delta\omega_e$ and ensure that the frequencies do not necessarily match with those used in the AKF, which are considered unknowns. Some under or overestimation in the estimated wave spectrum was noticed due to the large number of parameters to be estimated. A potential solution to address this, and a plan for future work, is to integrate other sensor sources such as radar data, which can provide accurate directional estimates. This can help to reduce the number of directions, thereby decreasing the number of states to be estimated.

Another important point to address in the future is the inclusion of non-linearities. The proposed method was tested using simulated motion responses generated using the RAO model, which is based on linear assumptions. As a result, nonlinear effects were not included in the motion response generation. Additionally, AKF used in this study is also based on linear assumptions (the measurement model derived from the RAO model). This means that potential nonlinearities, especially in large waves, extreme sea conditions, or under significant forward speed, may affect the accuracy of sea state estimation. The proposed method has been validated for small to moderate wave amplitudes, where the linear assumptions of the RAO apply. This restriction should be taken into account, and future research could include nonlinear effects via more modern techniques, e.g., by replacing the linear RAO model with a nonlinear unified state-space model [43], which explicitly accounts for these effects. Additionally, employing nonlinear filtering techniques, such as the Extended or Unscented Kalman Filter, could provide a more accurate estimation by handling the nonlinearities' effect. Regardless, it is important to remember the possible limitations stemming from this linear RAO assumption when implementing this or other model-based SAWB method. In the future, the proposed method will also be evaluated using real data collected from onboard motion sensors to assess its effectiveness in maritime conditions where nonlinearities are expected to play an important role.

Despite these points for future work, overall, the proposed method provides promising results for accurate time-domain estimation of a wave spectrum based on ship motion measurements with varying forward speed, enabling wave estimation that reflects real-world conditions. With the established time-domain approach presented here, further advantages of time domain estimation (e.g., sensor fusion, real-time estimation, consideration of other non-stationary and non-linear conditions) can be leveraged for improved sea state estimation.

CRediT authorship contribution statement

R. Bourkaib: Writing – original draft, Validation, Methodology, Investigation, Conceptualization. **M. Kok:** Writing – review & editing, Supervision, Funding acquisition, Conceptualization. **H.C. Seyffert:** Writing – review & editing, Supervision, Funding acquisition, Conceptualization.

Declaration of competing interest

The authors declare that they have no known competing financial interests or personal relationships that could have appeared to influence the work reported in this paper.

Acknowledgments

This publication is part of the project "FUSION: Smart Sensing for Informed Maintenance & Optimized Naval Design" (project number KICH1.VE-02.20.010) of the research programme "Maritime High-tech for safer seas" which is (partly) financed by the Dutch Research Council (NWO). The authors also gratefully acknowledge support from the FReady (Fleet Ready combination of physical virtual hull structure monitoring) JIP. The authors further appreciate the thoughtful and thorough comments from the anonymous reviewers.

Data availability

The authors do not have permission to share the data used in the case study, but the accompanying code can be accessed at 10.4121/d6e3306a-daca-4d2b-9d64-89f20e0eba5a.

References

[1] K. Lindemann, J. Odland, J. Strengtheagen, On the application of hull surveillance systems for increased safety and improved structural utilization in rough weather, Trans. Soc. Nav. Archit. Mar. Eng. (1977).

[2] F.W. Debord, B. Hennessy, Development of a Generalized Onboard Response Monitoring System, Technical Report SSC-349, Ship Structure Committee, 1990.

[3] U.D. Nielsen, H.B. Bingham, A.H. Brodtkorb, T. Iseki, J.J. Jensen, M. Mittendorf, R.E.G. Mounet, Y. Shao, G. Storhaug, A.J. Sørensen, T. Takami, Estimating waves via measured ship responses, Sci. Rep. (2023) http://dx.doi.org/10.1038/s41598-023-44552-2.

[4] K. Takekuma, T. Takahashi, On the evaluation of sea spectra based on the measured ship motions, Trans. West- Jpn. Soc. Nav. Archit. (1973) URL https://api.semanticscholar.org/CorpusID:119009920.

[5] O. Waals, A. Aalbers, J. Pinkster, Maximum likelihood method as a means to estimate the directional wave spectrum and the mean wave drift force on a dynamically positioned vessel, in: 21st International Conference on Offshore Mechanics and Arctic Engineering, Conference Publisher, 2002, http://dx.doi.org/10.1115/OMAE2002-28560.

[6] P. Naaijen, Deterministic Prediction of Waves and Wave Induced Vessel Motions. Future Telling by Using Nautical Radar as a Remote Wave Sensor (Ph.D. thesis), Delft University of Technology, 2017, http://dx.doi.org/10.4233/uuid:49bf7c26-e260-448a-b94a-5fcb038fa602.

[7] U.D. Nielsen, A concise account of techniques available for shipboard sea state estimation, Ocean Eng. (2017) http://dx.doi.org/10.1016/j.oceaneng.2016.11.035.

[8] J. Hua, M. Palmquist, Wave estimation through ship motion measurement, in: Engineering, Environmental Science, 1994, URL https://api.semanticscholar.org/CorpusID:126560733.

[9] T. Iseki, D. Terada, Bayesian estimation of directional wave spectra for ship guidance system, Int. J. Offshore Polar Eng. (2002) arXiv:https://onepetro.org/IJOPE/article-pdf/2181396/isope-02-12-1-025.pdf.

[10] U.D. Nielsen, Estimations of on-site directional wave spectra from measured ship responses, Mar. Struct. (2006) http://dx.doi.org/10.1016/j.marstruc.2006.06.001.

[11] R. Pascoal, C. Guedes Soares, A.J. Sørensen, Ocean wave spectral estimation using vessel wave frequency motions, J. Offshore Mech. Arct. Eng. (2006) http://dx.doi.org/10.1115/1.2426986.

[12] N. Montazeri, U. Nielsen, J. Jensen, Selection of the optimum combination of responses for wave buoy analogy - an approach based on local sensitivity analysis, in: U. Dam Nielsen, J. Juncher Jensen (Eds.), Proceedings of the 13th International Symposium on PRActical Design of Ships and Other Floating Structures, PRADS'2016, Technical University of Denmark, 2016.

[13] U.D. Nielsen, J. Dietz, Ocean wave spectrum estimation using measured vessel motions from an in-service container ship, Mar. Struct. (2020) http://dx.doi.org/10.1016/j.marstruc.2019.102682.

[14] A.H. Brodtkorb, U.D. Nielsen, Automatic sea state estimation with online trust measure based on ship response measurements, Control Eng. Pract. (2023) http://dx.doi.org/10.1016/j.conengprac.2022.105375.

[15] T. Iseki, U. Nielsen, Study on short-term variability of ship responses in waves, in: Proceedings of the 131st Conference of Japan Institute of Navigation, Japan Institute of Navigation, 2014.

[16] T. Kawai, Y. Kawamura, T. Okada, T. Mitsuyuki, X. Chen, Sea state estimation using monitoring data by convolutional neural network (CNN), J. Mar. Sci. Technol. (2021).

[17] G.A. Bisinotto, P.C. de Mello, F.G. Cozman, E.A. Tannuri, Motion-based wave inference with neural networks: Transfer learning from numerical simulation to experimental data, J. Offshore Mech. Arct. Eng. (2024) http://dx.doi.org/10.1115/1.4064618.

[18] T. Scholcz, B. Mak, Ship as a wave buoy: Estimating full directional wave spectra from in-service ship motion measurements using deep learning, Present. Int. Conf. Ocean. Offshore Arct. Eng. (2020) http://dx.doi.org/10.1115/OMAE2020-18783.

[19] N. Long, D. Sgarioto, M. Garratt, K. Sammut, Response component analysis for sea state estimation using artificial neural networks and vessel response spectral data, Appl. Ocean Res. (2022) http://dx.doi.org/10.1016/j.apor.2022.103320.

[20] M. Mittendorf, U. Nielsen, H. Bingham, G. Storhaug, Sea state identification using machine learning—A comparative study based on in-service data from a container vessel, Mar. Struct. (2022) http://dx.doi.org/10.1016/j.marstruc.2022.103274.

[21] D.J. Belleter, R. Galeazzi, T.I. Fossen, Experimental verification of a global exponential stable nonlinear wave encounter frequency estimator, Ocean Eng. (2015) http://dx.doi.org/10.1016/j.oceaneng.2014.12.030.

[22] U.D. Nielsen, R. Galeazzi, A.H. Brodtkorb, Evaluation of shipboard wave estimation techniques through model-scale experiments, in: OCEANS 2016 - Shanghai, 2016, http://dx.doi.org/10.1109/OCEANSAP.2016.7485701.

[23] R. Pascoal, C. Guedes Soares, Kalman filtering of vessel motions for ocean wave directional spectrum estimation, Ocean Eng. (2009) http://dx.doi.org/10.1016/j.oceaneng.2009.01.013.

[24] H. Kim, J. Park, C. Jin, M. Kim, D. Lee, Real-time inverse estimation of multi-directional random waves from vessel-motion sensors using Kalman filter, Ocean Eng. (2023) http://dx.doi.org/10.1016/j.oceaneng.2023.114501.

[25] Y. Komoriyama, K. Iijima, A. Tatsumi, M. Fujikubo, Identification of wave profiles encountered by a ship with no forward speed using Kalman filter technique and validation by tank tests - long-crested irregular wave case -, Ocean Eng. (2023) http://dx.doi.org/10.1016/j.oceaneng.2023.113627.

[26] Y. Komoriyama, K. Iijima, H. Houtani, A. Tatsumi, M. Fujikubo, Kalman filter technique for estimating encountered wave profiles and unmeasured ship responses using measurement data in short-crested irregular waves, Appl. Ocean Res. (2025) http://dx.doi.org/10.1016/j.apor.2025.104453.

[27] U.D. Nielsen, A.H. Brodtkorb, A.J. Sørensen, A brute-force spectral approach for wave estimation using measured vessel motions, Mar. Struct. (2018) http://dx.doi.org/10.1016/j.marstruc.2018.03.011.

[28] H. Majidian, L. Wang, H. Enshaei, Part a: A review of the real-time sea-state estimation, using wave buoy analogy, Ocean Eng. (2022) http://dx.doi.org/10.1016/j.oceaneng.2022.111684.

[29] H. Majidian, L. Wang, H. Enshaei, Part. B: A review of the real-time sea-state estimation, using wave buoy analogy; a decuple benchmark and future outlook, Ocean Eng. (2022) http://dx.doi.org/10.1016/j.oceaneng.2022.111020.

[30] U.D. Nielsen, M. Mittendorf, Y. Shao, G. Storhaug, Wave spectrum estimation conditioned on machine learning-based output using the wave buoy analogy, Mar. Struct. (2023) http://dx.doi.org/10.1016/j.marstruc.2023.103470.

[31] M. Longuet-Higgins, D. Cartwright, N. Smith, Observations of the directional spectrum of sea waves using the motions of a floating buoy, Ocean. Wave Spectra (1961).

[32] L.H. Holthuijsen, Waves in Oceanic and Coastal Waters, Cambridge University Press, 2007.

[33] U.D. Nielsen, Transformation of a wave energy spectrum from encounter to absolute domain when observing from an advancing ship, Appl. Ocean Res. (2017) http://dx.doi.org/10.1016/j.apor.2017.10.011.

[34] S. Akhlaghi, N. Zhou, Z. Huang, Adaptive adjustment of noise covariance in Kalman filter for dynamic state estimation, in: 2017 IEEE Power & Energy Society General Meeting, 2017, pp. 1–5, http://dx.doi.org/10.1109/PESGM.2017.8273755.

[35] R. Pascoal, L. Perera, C. Guedes Soares, Estimation of directional sea spectra from ship motions in sea trials, Ocean Eng. (2017) http://dx.doi.org/10.1016/j.oceaneng.2017.01.020.

[36] I. Drummen, L. Rogers, A. Benhamou, R. Hageman, K. Stambaugh, Hull Structure Monitoring of a New Class of US Coast Guard Cutters, ASNE- Technology, Systems & Ships, Wash. DC, USA, 2019.

[37] K. Stambaugh, I. Drummen, R. Hageman, I. Thompson, Hull Structural Monitoring of USCG Cutters to support Long Term Maintenance Decisions, ASNE- TSS, Wash. DC, USA, June 2019.

[38] R. Pascoal, C. Guedes Soares, Non-parametric wave spectral estimation using vessel motions, Appl. Ocean Res. (2008) http://dx.doi.org/10.1016/j.apor.2008.03.003.

[39] E. Jefferys, Directional seas should be ergodic, Appl. Ocean Res. (1987) http://dx.doi.org/10.1016/0141-1187(87)90001-0.

[40] T. Duarte, S. Gueydon, J. Jonkman, A. Sarmento, Computation of wave loads under multidirectional sea states for floating offshore wind turbines, in: International Conference on Offshore Mechanics and Arctic Engineering, 2014, http://dx.doi.org/10.1115/OMAE2014-24148.

[41] K. Hasselmann, T. Barnett, E. Bouws, H. Carlson, D. Cartwright, K. Enke, J. Ewing, H. Gienapp, D. Hasselmann, P. Kruseman, A. Meerburg, P. Muller, D. Olbers, K. Richter, W. Sell, H. Walden, Measurements of wind-wave growth and swell decay during the joint North Sea wave project (JONSWAP), Deut. Hydrogr. Z. 8 (1973) 1–95.

[42] U.D. Nielsen, Introducing two hyperparameters in Bayesian estimation of wave spectra, Probabilistic Eng. Mech. (2008) http://dx.doi.org/10.1016/j.probengmech.2007.10.007.

[43] R. Sandeepkumar, S. Rajendran, R. Mohan, A. Pascoal, A unified ship manoeuvring model with a nonlinear model predictive controller for path following in regular waves, Ocean Eng. (2022) http://dx.doi.org/10.1016/j.oceaneng.2021.110165.